# Reversed hysteresis during CO oxidation over $Pd_{75}Ag_{25}(100)$

Vasco R. Fernandes,[1†] Maxime Van den Bossche,[2†] Jan Knudsen,[3,4] Mari H. Farstad,[1] Johan Gustafson,[4] Hilde J. Venvik,[5] Henrik Grönbeck,[2*] and Anne Borg[1*]

[1]*Department of Physics, Norwegian University of Science and Technology, NO-7491 Trondheim, Norway,* [2]*Competence Centre for Catalysis and Department of Physics, Chalmers University of Technology, SE-41296 Göteborg, Sweden,* [3]*MAX IV Laboratory, Lund University, Box 118, SE-221 00 Lund, Sweden,* [4]*Division of Synchrotron Radiation Research, Lund Univ., Box 117, SE-221 00 Lund, Sweden,* [5]*Department of Chemical Engineering, Norwegian University of Science and Technology, NO-7491 Trondheim, Norway*

E-mail: ghj@chalmers.se;anne.borg@ntnu.no

*To whom correspondence should be addressed

† Equal contributions

**Abstract**

CO oxidation over Pd(100) and $Pd_{75}Ag_{25}$(100) has been investigated by a combination of near-ambient pressure X-ray photoelectron spectroscopy, quadrupole mass spectrometry, density functional theory calculations and micro-kinetic modeling. For both surfaces, hysteresis is observed in the $CO_2$ formation during heating and cooling cycles. Whereas normal hysteresis with higher light-off temperature than extinction temperature is present for Pd(100), reversed hysteresis is observed for $Pd_{75}Ag_{25}$(100). The reversed hysteresis can be explained from dynamic changes in the surface composition. At the beginning of the heating ramp, the surface is rich in palladium which gives a CO coverage that poisons the surface until the desorption rate becomes sufficiently high. The thermodynamic preference for an Ag rich surface in the absence of adsorbates promotes diffusion of Ag from the bulk to the surface as CO desorbs. During the cooling ramp, an appreciable surface coverage is reached at temperatures too low for efficient diffusion of Ag back into the bulk. The high concentration of Ag in the surface leads to a high extinction temperature and, consequently, the reversed hysteresis.

**Keywords:** CO oxidation, Pd(100), $Pd_{75}Ag_{25}$(100), hysteresis, APXPS, DFT, kinetic modeling

# Introduction

The possibility to synthesize bimetallic systems opens up new routes to engineer catalysts with enhanced properties. It has already been demonstrated that the selectivity and activity in this way can be modified for important reactions such as catalytic reforming,[1] oxidation[2] and electrochemical oxygen reduction.[3]

Monometallic palladium is a versatile oxidation catalyst which is used in various applications such as CO removal from car exhaust[4,5] and total oxidation of hydrocarbons.[6–9] For palladium, alloying with noble metals such as Cu and Ag has been shown to alter adsorption properties related to hydrogen bulk diffusion.[10] However, the mere alloying could be advantageous as it reduces the amount of the precious metal yet retaining the activity.

The use of bimetallic systems for reactions adds additional complexity with respect to reaction dynamics. For nanoparticles and extended surfaces, it has been demonstrated that reactions may drive restructuring and segregation. In the case of PdAg alloys, silver segregation to the surface under ultra high vacuum (UHV) conditions has been observed experimentally,[11,12] and predicted from calculations.[13–19] The segregation originates from the lower surface energy of Ag as compared to Pd[15,17,20,21] and from the reduction of stress owing to the slightly larger Ag atoms. As a result of differences in chemisorption energies of interacting molecules,[22,23] experiments have shown adsorbate-induced segregation of Pd in PdAg alloys upon adsorption of oxygen[24,25] and hydrogen.[26] We have, for example, recently reported that the $Pd_{75}Ag_{25}(100)$ surface forms a $(\sqrt{5} \times \sqrt{5})R27°$ surface oxide (henceforth denoted $\sqrt{5}$) similar to the one observed on Pd(100).[25] In this case, Pd segregates to the surface to form the oxide structure and an enrichment of Ag is observed in the interface layer between the surface oxide and the $Pd_{75}Ag_{25}$ bulk. Theoretical studies also find adsorbate-induced segregation as a result of oxygen,[14,27] hydrogen,[19,27–29] and CO[27] adsorption.

It has been reported that surface oxides formed on Pd surfaces at near ambient pressure conditions are more active in oxidation reactions than the metal surface covered with chemisorbed oxygen.[30–40] In the case of Pd(100), it has been shown experimentally that

the higher activity of this surface towards CO oxidation at these conditions coincides with the presence of the $\sqrt{5}$ surface oxide.[30,32,35,38,39,41] Kinetic Monte-Carlo simulations support the view that a surface oxide on Pd(100) could be responsible for increased reactivity.[42,43] Although some studies indicate a chemisorbed oxygen phase as the active surface,[32,44] the emergent trend points to the surface oxide[33,35,38,39] as the most active phase under oxygen rich conditions. The CO oxidation reaction under ultrahigh vacuum (UHV) conditions can be described by a Langmuir-Hinshelwood mechanism.[45–49] Under more realistic conditions, several studies indicate that the mechanism is of Mars van Krevelen type, where the catalyst surface is oxidized and gas phase CO interacts with the oxide to form $CO_2$.[30–33,35,37–40,50]

In the present work, we have investigated the influence of Ag as alloying element in Pd catalysts through comparison of the CO oxidation reaction over Pd(100) and $Pd_{75}Ag_{25}$(100). Near ambient pressure X-ray photoelectron spectroscopy (NAP-XPS) and quadrupole mass spectrometry (QMS) measurements have been compared to density functional theory and micro-kinetic modeling. In particular, hysteresis effects during temperature cycling will be addressed.

# Experimental Methods

Pd(100) and $Pd_{75}Ag_{25}$(100) single crystals were cleaned by cycles of sputtering, oxygen treatment and annealing to 705°C for Pd(100) and 625°C for $Pd_{75}Ag_{25}$(100). Temperatures were measured with a type K thermocouple spotwelded to the edge of the crystal. The surface quality was evaluated by low energy electron diffraction (LEED), revealing well defined surfaces, and by XPS measurement of the C 1$s$ and S 2$p$ core level spectra, where no traces of these impurities were observed.

NAP-XPS measurements were performed at beam line I511 of the MAX IV Laboratory.[51] This beam line was equipped with a SPECS PHOIBOS 150 NAP analyzer for near ambient pressure measurements and a reaction cell, which was filled with gases during experiments.

The NAP-XPS data were recorded *in situ* at gas pressures of about 0.7 mbar. Total gas flows of 2.0-3.0 $cm^3$/min were applied. The gas composition at the exhaust of the reaction cell was analyzed using a QMS connected to the gas exit lines via a leak valve. The QMS instrument was a Dycor LC-D Residual Gas Analyzer from AMTEK. The oxidation experiments were carried out by introducing $O_2$:CO gases at a ratio 10:1 and varying the sample temperature. NAP-XPS, QMS, and temperature data were collected continuously during the experiments.

O 1$s$, Ag 3$d_{5/2}$, Pd 3$d_{5/2}$, and C 1$s$ core level spectra were recorded at photon energies 650, 450, 400, and 380 eV, respectively. All spectra were measured at normal emission. The binding energy was calibrated by recording the Fermi edge immediately after the core level regions. Linear background subtraction was applied and Doniach-Sunjic line shapes used for fitting the spectra.[52]

# Computational Methods

The Density Functional Theory (DFT) was applied with the gradient corrected exchange-correlation functional according to Perdew, Burke and Ernzerhof (PBE).[53] The VASP code was used.[54–56] The one-electron Kohn-Sham orbitals were expanded in a plane wave basis set with a kinetic energy cutoff of 450 eV. PAW potentials were used to describe the interaction between the valence electrons and the core.[57,58] A p(2×2) surface cell was considered for Pd(100) and $Pd_{75}Ag_{25}$(100). The surface was modeled as a slab with five atomic layers. The slabs were separated by 12 Å in the direction normal to the surface. Reciprocal space integration over the Brillouin zone was approximated with finite sampling using a 6×6×1 Monkhorst-Pack grid.[59,60] Geometry optimizations were carried out keeping the two bottom layers fixed at bulk positions. The structures were considered relaxed when the largest force in the system was smaller than 0.01 eV/Å. Dimer calculations[61] were performed to obtain activation energies. The lattice constants for Pd and $Pd_{75}Ag_{25}$were calculated to be 3.95 and 4.02 Å, respectively, which is in good agreement with previous reports.[25] The surface slabs

for the alloy were constructed with the lattice constant of $Pd_{75}Ag_{25}$and a 3:1 stoichiometry in each layer.

The DFT results were used as input to a micro-kinetic model. The model is based on the conventional Langmuir-Hinshelwood mechanism for CO oxidation:

$$CO + * \rightleftharpoons CO* \quad (1)$$

$$O_2 + 2* \rightleftharpoons 2O* \quad (2)$$

$$CO* + O* \rightleftharpoons CO_2 + 2* \quad (3)$$

where $*$ corresponds to a surface site.

The corresponding rate equations with the coverages of CO ($\theta_{CO}$) and O ($\theta_O$) are approximated by:[62]

$$\frac{\partial \theta_{CO}}{dt} = s^0_{CO} p_{CO} k^a_{CO}(1-\theta^2_{CO}) - k^d_{CO}\theta_{CO} - k^r \theta_{CO}\theta_O \quad (4)$$

$$\frac{\partial \theta_O}{dt} = 2s^0_O p_{O_2} k^a_{O_2}(1-\theta_{CO}-\theta_O)^2 - 2k^d_{O_2}\theta^2_O - k^r \theta_{CO}\theta_O \quad (5)$$

$s^0_i$ and $p_i$ are sticking coefficients and partial pressures, respectively. The sticking coefficients over Pd were set to 0.4 and 0.7 for $O_2$ and CO, respectively.[63] On Ag, the sticking for $O_2$ (0.001) was taken from Ref.,[64] whereas the CO sticking coefficient was set to 0.1 as a reasonable estimate. It is assumed that oxygen does not influence the CO adsorption, whereas CO influences the oxygen adsorption. The corresponding rate constants are given by:

$$k^a_X = A_s/\sqrt{2\pi M k_B T} \quad (6)$$

$$k^d_{CO} = \nu^d_{CO} e^{-E^d_{CO}(1-\alpha\theta_{CO})/k_B T} \quad (7)$$

$$k^d_{O_2} = \nu^d_{O_2} e^{-E^d_{O_2}(1-\alpha\theta_O)/k_B T} \quad (8)$$

$$k^r = \nu^r e^{-E^r(1-\beta\theta_{CO})/k_B T} \quad (9)$$

Here, $A_s$ is the area of a site, $M$ is the mass of the molecule under consideration , $k_B$ the Boltzmann factor and $T$ the temperature. The desorption energies for $O_2$, CO and the reaction barrier are denoted $E^d_{CO}$, $E^d_{O_2}$ and $E^r$, respectively. Lateral adsorbate interactions are included through coverage dependent desorption and reaction energies, where $\alpha = 0.5$ and $\beta = 0.1$. The pre-exponential factors for desorption and reaction are set to $\nu^d_{CO} = 10^{15}$, $\nu^d_{O_2} = 10^{14}$ and $\nu^r = 10^{14}$ 1/s.

To allow for diffusion of Ag atoms during the reaction and a varying coverage of Ag atoms in the surface layer ($\theta_{Ag}$), the reaction kinetics are augmented by:

$$\frac{\partial \theta_{Ag}}{dt} = k^{diff}_{+}\theta^{bulk}_{Ag} - k^{diff}_{-}\theta^{surf}_{Ag} \tag{10}$$

$k^{diff}_{+}$ and $k^{diff}_{-}$ are the rate constants for diffusion to and from the surface layer, respectively. The pre-exponential factor for the rate constant is in this case set to $2.2 \times 10^{11}$ 1/s and an estimated value of 2.0 eV for Ag diffusion barrier in PdAg is applied.[65] Desorption and activation energies for any Ag coverage in the surface layer are obtained by linear interpolation between the calculated coverages (0, 0.25, 0.5 0.75 and 1).

In the present work, we have chosen to keep the kinetic model relatively simple. Regarding the surface composition, we have considered a homogeneous distribution of Pd and Ag atoms in the surface layer and neglected possible island formation. Moreover, in the surface kinetics, we have assumed temperature independent sticking coefficients, typical pre-exponential factors and simple coverage dependencies. Despite the limitations of the model, it contains the essential features that allow for a qualitative description. A sensitivity analysis of the results with respect to the chosen parameters shows that the kinetic behaviour over the two systems remains in qualitative agreement with the experiments over a range of parameters.[66]

# Results and discussion

## CO Oxidation over Pd(100)

In Fig. 1(a) *in situ* NAP-XPS measurements of the Pd $3d_{5/2}$ core level region along with QMS data for CO oxidation over Pd(100) under oxygen rich conditions ($O_2$:CO at ratio 10:1) are presented. The experiment was performed by ramping the temperature from 80°C to 230°C followed by ramping down to about 155°C. The total pressure was kept fixed at 0.7 mbar during the entire experiment. The Pd $3d_{5/2}$ core level spectrum obtained at 85°C (labeled 1), displayed in the lower panel of Fig. 1(b), comprises contributions from CO adsorbed in bridge sites (in grey) on the metallic surface at a binding energy of 335.5 eV and the Pd $3d_{5/2}$ bulk contribution at 334.8 eV (in blue). In the lower panel of Fig. 1(c), the spectrum of the O 1*s* region recorded at 110°C during a similar measurement series is displayed. The CO induced component (in grey) has a binding energy of 531.4 eV and the Pd $3p_{3/2}$ peak (in blue) has a binding energy of approximately 531.8 eV. Two components located at 537.0 eV and 538.1 eV are both assigned to molecular oxygen in the gas phase. The contribution from CO in the gas phase is expected at about 536.0 eV, but can not be easily discerned in the experimental spectrum and was therefore not included in the deconvolution. Only $CO_2$ from the residual gas in the QMS chamber is observed at this point.

The spectrum is changing as the temperature is increased. At 140°C, the $CO_2$ partial pressure, as recorded by QMS, starts to increase. The NAP-XPS data does not indicate changes in the surface species at this point, in line with previous observations.[30,37,38] Reaching a temperature of about 195°C, changes in the NAP-XPS spectra indicate altered Pd(100) surface chemistry. The Pd $3d_{5/2}$ core level spectrum measured at this stage, at temperature 210°C, including curve fitting, is displayed in the upper panel (labeled 2) of Fig. 1(b). The component assigned to adsorbed CO is no longer present. Instead, three peaks located at binding energies of 334.7 eV, 335.3 eV and 336.1 eV are observed, in addition to the Pd bulk feature. These three peaks are clear fingerprints of the $\sqrt{5}$ surface oxide on Pd(100)[67]

and originate from Pd at the interface between the $\sqrt{5}$ surface oxide (in orange) and surface oxide Pd atoms 2-fold (in yellow) and 4-fold (in green) coordinated with oxygen atoms, respectively.[67] The O 1*s* core level spectrum at this stage, measured at 210°C, including curve fitting, is displayed in the upper panel (labeled 2) of Fig. 1(c). The component due to adsorbed CO is no longer present. Instead, two peaks located at binding energies 528.8 eV and 529.5 eV (in pink) are observed, also being clear fingerprints of the $\sqrt{5}$ surface oxide on Pd(100),[67] and representing interface and surface oxygen atoms in the $\sqrt{5}$ surface oxide.[25] An additional peak at 535.4 eV (in purple) due to $CO_2$ in the gas phase is also observed. Moreover, the oxygen gas phase components are shifted by 0.5 eV to higher binding energies, as a consequence of a change in the work function of the sample. Simultaneously, the QMS data shows a high, steady production of $CO_2$. These observations are in line with previous reports, which show higher reactivity for CO oxidation when the Pd(100) surface is covered by the $\sqrt{5}$ surface oxide.[33,35,38,39] Further increase in temperature yields no notable changes in the surface reactivity, indicating that the reaction is mass transfer limited once the temperature of the highly reactive stage is reached.

Reducing the temperature yields a transition from the $\sqrt{5}$ surface oxide covered surface to a CO covered surface accompanied by extinction of the $CO_2$ production. The Pd $3d_{5/2}$ core level spectra reveal that the change in surface chemistry occurs at about 160°C, which is below the light-off temperature at about 195°C. This kind of hysteresis in the reaction kinetics is common for CO oxidation over Pd and Pt where the surface is CO-poisoned at low temperatures, see *e.g.* Ref.[63]

## CO Oxidation over $Pd_{75}Ag_{25}(100)$

Turning to $Pd_{75}Ag_{25}(100)$, the CO oxidation reaction over this surface was performed similarly to the CO oxidation over Pd(100). The results from the *in situ* NAP-XPS experiments monitoring the Pd $3d_{5/2}$ core level region, along with QMS measurements of $O_2$, CO and $CO_2$, conducted at an $O_2$:CO ratio of 10:1 at a total pressure of 0.7 mbar while ramping the

sample temperature from about 35°C up to 440°C and then cooling down to about 60°C are presented in Fig. 2(a). As in the case of Pd(100), at the initial stage, measured at 35°C, labeled 1 in Fig. 2(a), only $CO_2$ from the residual gas in the QMS chamber is observed. The NAP-XPS Pd $3d_{5/2}$ core level spectrum, shown in the lower panel (labeled 1) of Fig. 2(b), displays two main contributions, a CO induced component at a binding energy of 335.8 eV (in grey) and the $Pd_{75}Ag_{25}$bulk component at a binding energy of 334.8 eV (in blue). Noteworthy is the much weaker CO contribution for $Pd_{75}Ag_{25}(100)$ compared to Pd(100), showing that a significant amount of Ag is present in the outermost surface layer. The corresponding NAP-XPS O $1s$ core level spectrum, measured during a separate ramping series, shows three main contributions. The decomposition of the spectrum, displayed in the lower panel of Fig. 2(c), yields the same spectral components as for CO oxidation over Pd(100) in the low reactivity stage. The lower intensity of the CO contribution, at binding energy 530.5 eV (in grey), compared to the corresponding peak in Fig. 1(c), is in line with the trend seen from the Pd $3d_{5/2}$ spectra.

At a sample temperature of about 140°C, the $CO_2$ QMS signal increases. Raising the temperature further results in growing $CO_2$ production, with a high CO oxidation activity reached at about 230°C. Interestingly, and in contrast to the Pd(100) case, the NAP-XPS spectra of the Pd $3d_{5/2}$ region for $Pd_{75}Ag_{25}(100)$ do not show any signature of the $\sqrt{5}$ surface oxide and increasing the temperature does not change this picture. The $\sqrt{5}$ surface oxide on $Pd_{75}Ag_{25}(100)$ is characterized by two oxygen induced components in the Pd $3d_{5/2}$ core level spectrum at binding energies 336.1 eV (4-fold) and 335.3 eV (2-fold).[25] In the upper panel of Fig. 2(b) the fitted Pd $3d_{5/2}$ core level spectrum recorded at about 440°C is displayed (labeled 2). In addition to the $Pd_{75}Ag_{25}$bulk component, the spectrum reveals two contributions related to Pd atoms at the surface of $Pd_{75}Ag_{25}(100)$ (in brown), at binding energy 334.5 eV, and a $Pd_{75}Ag_{25}$alloy surface component (in pale blue) at about 335.2 eV.[68] The latter peak may also include a contribution from atomic oxygen adsorbed on the alloy surface. The corresponding O $1s$ core level spectrum measured at similar temperature during a separate

ramping series, displayed in the upper panel of Fig. 2(c) shows a component attributed to atomic oxygen at a binding energy of 529.4 eV (in pink). The slight shift in the Pd $3p_{3/2}$ core level position may be related to a difference in the surface chemistry at low and high temperatures. The changes in the relative intensities of the peaks from gas phase molecular oxygen (in red) and the Pd $3p_{3/2}$ peaks in the lower and upper panels of Fig. 2(c) are primarily related to thermal expansion during the experiments, changing the distance between the sample and electron analyzer entrance, thus affecting the gas volume measured in front of the sample surface. A component due to gas phase $CO_2$ (in purple) is seen in Fig. 2(c) in addition to the peaks due to gas phase oxygen. Only a minor shift of 0.1 eV in the binding energies of the gas phase contributions are seen between the inactive and active stages of the CO oxidation reaction over $Pd_{75}Ag_{25}(100)$, indicating minor changes in the sample work function and the surface chemistry.

Interestingly, as the temperature is increased from 230°C to 430°C, the $CO_2$ partial pressure as measured by QMS decreases and, correspondingly, the CO partial pressure increases. Decreasing the temperature from 430°C to 260°C leads to recovery of the $CO_2$ production, although to a smaller extent than the maximum $CO_2$ production. Further reduction in temperature leads to the conditions (at approximately 200°C) where CO again covers the surface and inhibits the reaction.

The high activity regime for the catalytic CO oxidation on $Pd_{75}Ag_{25}(100)$ shows a significant difference in surface chemistry as compared to Pd(100). Whereas a $\sqrt{5}$ surface oxide is observed on Pd(100), only chemisorbed oxygen is present on $Pd_{75}Ag_{25}(100)$ in the high activity phase. Noteworthy is also the temperature dependence of the $CO_2$ signal for $Pd_{75}Ag_{25}(100)$ in the high activity regime, which decreases with increasing temperature. Furthermore, the extinction temperature for $Pd_{75}Ag_{25}(100)$ is higher that the light-off temperature. Thus, the hysteresis is reversed as compared to Pd(100).

## Theoretical analysis of the CO oxidation kinetics

To elucidate the experimental findings, we performed DFT calculations coupled to a mean field micro-kinetic analysis. CO oxidation over Pd(100) and $Pd_{75}Ag_{25}$(100) was investigated by calculations of CO and O adsorption energies together with the activation energy to form $CO_2$ (Table 1). As the surface composition of the alloy may vary during the experiments, different compositions of the top-most layer were considered.

The results for Pd(100) are in good agreement with previous reports.[69] Atomic oxygen is preferably adsorbed in a hollow position, whereas CO is adsorbed in a bridge position. The activation energy is calculated to be 0.81 eV and both O and CO are close to bridge positions in the transition state (TS) where $CO_2$ is formed over the hollow site.

The preferred adsorption sites and geometry of the TS on an all-Pd layer supported on $Pd_3Ag$ bulk are similar to that of Pd(100). However, the energetics is different with higher adsorption energies and a higher activation energy. The difference is rationalized by the 2.4% expansion of the surface cell as compared to Pd(100).[70] Having a $Pd_3Ag$ composition in the surface of the alloy does not change the adsorption energies. The activation energy is, however, increased to as much as 1.25 eV as a consequence of site competition where CO is close to an atop site during the TS. (The hollow site is preferred by $\sim$0.4 eV over atop on Pd(100)[71]). Increasing the Ag content in the top-most layer yields a change in the stable adsorption site for CO from bridge to atop. The adsorption energies are reduced for higher Ag content which results in reduced activation energies. The character of the TS is changing in the case of $PdAg_3$ in the sense that oxygen is close to the hollow site at the TS. The bond distances at the transition states are modified moderately and monotonically as a function of surface composition. The C-O bond is 1.18 Å over Pd(100) and Pd supported on $Pd_3Ag$, whereas it is 1.16 Å over $Ag_4/Pd_3Ag$. The O-CO distance is changing somewhat more, it is 1.98 Å over Pd(100) and Pd supported on $Pd_3Ag$ and 2.08 Å over $Ag_4/Pd_3Ag$.

Computational (a and b) and experimental (c and d) kinetics during temperature ramps of the CO oxidation reaction over Pd(100) and PdAg(100) are shown in Fig. 3. As is evident

Table 1: Adsorption energies of O [$E_a$(O)] and CO [$E_a$(CO)] together with the reaction activation energy $E^r$. The preferred adsorption site and the structural character of the transition state is given in parenthesis [hollow (h), bridge (b), and atop (t)]. Energies are in eV and the adsorption energies are calculated with respect to CO and $O_2$ in the gas phase, respectively. The barrier heights are calculated with respect to CO and O in separate unit cells.

| Surface | Bulk | $E_a$(O) | $E_a$(CO) | $E^r$ |
|---|---|---|---|---|
| $Pd_4$ | $Pd_4$ | -1.27 (h) | -1.85 (b) | 0.81 (b-b) |
| $Pd_4Ag_0$ | $Pd_3Ag$ | -1.34 (h) | -1.92 (b) | 0.84 (b-b) |
| $Pd_3Ag_1$ | $Pd_3Ag$ | -1.36 (h) | -1.94 (b) | 1.25 (b-t) |
| $Pd_2Ag_2$ | $Pd_3Ag$ | -1.05 (h) | -1.47 (t) | 0.90 (b-t) |
| $Pd_1Ag_3$ | $Pd_3Ag$ | -0.81 (h) | -1.48 (t) | 1.05 (h-t) |
| $Pd_0Ag_4$ | $Pd_3Ag$ | -0.54 (h) | -0.29 (t) | 0.06 (h-t) |

from comparing the experimental results for Pd(100) (c) and $Pd_{75}Ag_{25}$(100) (d), is that while the reaction is mass transfer limited on Pd(100) this is not the case for $Pd_{75}Ag_{25}$(100), a finding that can be rationalized by a combination of adsorption and segregation properties of the $Pd_{75}Ag_{25}$(100) surface as discussed below. Experimentally, the reaction over Pd(100) lights off at about 195°C when the temperature is ramped up. During the temperature ramp from high to low temperatures, the reaction is sustained until 150°C. Thus, the reaction has a bi-stability window of about 50°C. The calculations reproduce the experiments although the range of the bi-stability region is somewhat overestimated.

An initial composition of $Pd_2Ag_2$ was chosen for the simulations of the CO oxidation kinetics over the alloy. The composition was selected based on the fact that the experiments indicate a significant amount of Ag in the outermost surface layer. This is illustrated by the spectral strengths of the CO induced contributions in the lower panel of Fig. 2(b) and Fig. 2(c) compared to the corresponding spectra for Pd(100) shown in Fig. 1(b) and Fig. 1(c). The bi-stability kinetics are very different on the alloy as compared to the monometallic Pd. For $Pd_{75}Ag_{25}$(100), the experimental light-off is at 200°C, whereas the extinction is at approximately 225°C. Thus, the bi-stability is reversed with respect to the Pd(100) case. The simulations reproduce closely the reversed kinetics together with the temperature interval of the bi-stability.

The simulations provide a possibility to rationalize the reason for the reversed hysteresis. The CO adsorption energy is at this coverage -1.47 eV and the activation energy 0.91 eV. Increasing the temperature will monotonically lower the CO coverage due to thermal desorption. The calculations show that the CO coverage is about 0.5 ML at the light-off and close to zero at 450°C. The O coverage is 0.25 ML at light-off and about 0.05 at 450°C. Above the light-off temperature, the activity is reduced as a consequence of lower CO and O surface coverages. This is in agreement with the experimental results shown in Fig. 2(a). The low total coverage of surface species at high temperatures makes it energetically preferable to have Ag enrichment of the surface. As the high temperature allows for Ag diffusion, the surface composition is changed to $Pd_1Ag_3$ at 500°C. The enrichment of Ag in the surface layer is an additional reason for the reduction of the activity after light-off as the activity of Ag for CO oxidation is lower than Pd. With a $Pd_1Ag_3$ composition in the surface, the O adsorption energy is reduced to -0.81 eV, whereas the CO adsorption energy is unchanged and the activation energy for $CO_2$ formation is increased to 1.05 eV. These are changes that make the extinction of the reaction to occur at higher temperatures than the light-off. As the temperature is ramped down, the Ag enriched surface remains despite the fact that the adsorbate coverages increase. During this phase, the temperature is not sufficiently high to allow for Ag diffusion back to the bulk of the system. This conjecture is supported by NAP-XPS measurements (not shown), recorded at 450 eV, of a spectral region covering both the Ag 3d and the Pd 3d core levels before and after a ramping cycle. These spectra reveal a slightly higher Ag/Pd ratio after completion of a ramp from low to high and back down to low temperature, caused by a net segregation of Ag to the surface during the ramping series.

Hysteresis where the light-off temperature is higher than the extinction temperature is often observed and CO oxidation over Pd and Pt surfaces are archetypical examples. The underlying mechanism for this phenomenon is the existence of a kinetic regime where the system can have a steady state with either high or low activity. Reversed hysteresis is far less documented. Previous examples are NO oxidation over Pt[72,73] and CO oxidation over Pt

in the presence of $C_3H_6$.[74] The mechanism for the reversed hysteresis during NO oxidation over Pt was suggested to be the reversible oxidation of Pt by $NO_2$. This mechanism is, thus, similar in nature to what we have observed for CO oxidation over $Pd_{75}Ag_{25}(100)$ in the sense that it originates from a change in the composition of the catalyst. In the case of CO oxidation in the presence of $C_3H_6$,[74] the mechanism appears to be different, as the lower activity during the extinction was suggested to be due to the formation of $C_3H_6$ oxidation intermediates which block sites for CO adsorption.

# Conclusions

Comparing the catalytic oxidation of CO over Pd(100) and $Pd_{75}Ag_{25}(100)$ surfaces under oxygen rich conditions at near-ambient pressures clearly shows that Ag affects the reaction kinetics dramatically. Bi-stable reaction kinetics are observed on both surfaces, however, with different character. On Pd(100), the bi-stable hysteresis is of the usual type with a light-off temperature that is higher than the extinction temperature, whereas the hysteresis is reversed on $Pd_{75}Ag_{25}(100)$. The origin of the reversed hysteresis was traced back to Ag segregation to the surface for the alloy. The alloy surface is at low temperatures covered with CO which stabilized Pd in the topmost layer. As the temperature is increased and the CO poisoning is lifted, Ag diffuses to the surface. With a higher Ag concentration in the surface, the activation energy increases, whereas the oxygen adsorption energy decreases. These are the changes that cause the extinction temperature to be higher than the light-off temperature. Another difference between the two surfaces is the state of the surface in the high activity regime. The Pd(100) surface is during the high activity covered with the $\sqrt{5}$ surface oxide whereas the $Pd_{75}Ag_{25}(100)$ surface is metallic with adsorbed oxygen. Consequently, the CO oxidation reaction proceeds via a Mars van Krevelen mechanism on Pd(100) while a Langmuir-Hinchelwood mechanism applies for $Pd_{75}Ag_{25}(100)$. The present study underlines the dynamic character of alloy surfaces and demonstrates the capability

of NAP-XPS in combination with mass spectrometry and DFT-based modeling to unravel atomistic details during surface reactions.

## Acknowledgement

Financial support from Research Council of Norway (Project No. 138368/V30), NordForsk (Grant no. 40521), Swedish Research Council (Grant no. 2011-3532 and 621-2014-4708), and Chalmers Area of Advance Nanoscience and Nanotechnology is greatly acknowledged. We thank the staff at the MAX IV Laboratory for excellent support. The calculations have been performed at C3SE, Göteborg, through a SNIC grant.

## References

(1) Sankar, M.; Dimitratos, N.; Miedziak, P. J.; Wells, P. P.; Kiely, C. J.; Hutchings, G. J. *Chem. Soc. Rev* **2012**, *41*, 8099.

(2) Tao, F.; Grass, M. E.; Zhang, Y.; Butcher, D. R.; Renzas, J. R.; Liu, Z.; Chung, J. Y.; Mun, B. S.; Salmeron, M.; Somorjai, G. A. *Science* **2008**, *322*, 932.

(3) Escudero-Escribano, M.; Verdaguer-Casadevall, A.; Malacrida, P.; Gronbjerg, U.; Knudsen, B. P.; Jepsen, A. K.; Rossmeisl, J.; Stephens, I. E. L.; Chorkendorff, I. *J. Am. Chem. Soc.* **2012**, *134*, 16476.

(4) Heck, R.; Farrauto, R. *Catalytic Air Pollution Control: Commercial Technology*, 3rd ed.; Van Nostrand Reinhold, 2009.

(5) Centi, G. *J. Mol. Catal. A: Chem.* **2001**, *173*, 287.

(6) Henry, P. *Palladium Catalyzed Oxidation of Hydrocarbons*; Springer, 1980.

(7) Warren, B. K.; Oyama, S. T. *Heterogeneous hydrocarbon oxidation*; American Chemical Society, 1996.

(8) Ciuparu, D.; Lyubovsky, M. R.; Altman, E.; Pfefferle, L. D.; Datye, A. *Catal. Rev.* **2002**, *44*, 593.

(9) Gélin, P.; Primet, M. *Appl. Catal. B* **2002**, *39*, 1.

(10) Semidey-Flecha, L.; Sholl, D. S. *J. Chem. Phys.* **2008**, *128*, 144701.

(11) Wouda, P. T.; Schmid, M.; Nieuwenhuys, B.; Varga, P. *Surf. Sci.* **1998**, *417*, 292.

(12) Marten, T.; Hellman, O.; Ruban, A. V.; Olovsson, W.; Kramer, C.; Godowski, J. P.; Bech, L.; Li, Z.; Onsgaard, J.; Abrikosov, I. A. *Phys. Rev. B* **2008**, *77*, 125406.

(13) Kitchin, J. R.; Reuter, K.; Scheffler, M. *Phys. Rev. B* **2008**, *77*, 075437.

(14) Khanra, B. C.; Menon, M. *Physica B* **2000**, *291*, 368.

(15) Ropo, M.; Kokko, K.; Vitos, L.; Kollár, J. *Phys. Rev. B* **2005**, *71*, 045411.

(16) Ropo, M. *Phys. Rev. B* **2006**, *74*, 195401.

(17) Løvvik, O. M. *Surf. Sci.* **2005**, *583*, 100.

(18) Kim, H. Y.; Kim, H. G.; Ryu, J. H.; Lee, H. M. *Phys. Rev. B* **2007**, *75*, 212105.

(19) González, S.; Neyman, K. M.; Shaikhutdinov, S.; Freund, H.-J.; Illas, F. *J. Phys. Chem. C* **2007**, *111*, 6852.

(20) Vitos, L.; Ruban, A. V.; Skriver, H. L.; Kollár, J. *Surf. Sci.* **1998**, *411*, 186.

(21) Ruban, A. V.; Simak, S. I.; Korzhavyi, P. A.; Johansson, B. *Phys. Rev. B* **2007**, *75*, 054113.

(22) Tománek, D.; Mukherjee, S.; Kumar, V.; Bennemann, K. H. *Surf. Sci.* **1982**, *114*, 11.

(23) van den Oetelaar, L. C. A.; Nooij, O. W.; Oerlemans, S.; Denier van der Gon, A. W.; Brongersma, H. H.; Lefferts, L.; Roosenbrand, A. G.; van Veen, J. A. R. *J. Phys. Chem. B* **1998**, *102*, 3445.

(24) Wouda, P. T.; Schmid, M.; Nieuwenhuys, B. E.; Varga, P. *Surf. Sci.* **1999**, *423*, 229.

(25) Walle, L. E.; Grönbeck, H.; Fernandes, V. R.; Blomberg, S.; Farstad, M. H.; Schulte, K.; Gustafson, J.; Andersen, J. N.; Lundgren, E.; Borg, A. *Surf. Sci.* **2012**, *606*, 1777.

(26) Shu, J.; Bongondo, B. E. W.; Grandjean, B. P. A.; Adnot, A.; Kaliaguine, S. *Surf. Sci.* **1993**, *291*, 129.

(27) Svenum, I.-H.; Herron, J. A.; Mavrikakis, M.; Venvik, H. J. *Catal. Today* **2012**, *193*, 111.

(28) Løvvik, O. M.; Olsen, R. A. *J. Chem. Phys* **2003**, *118*, 3268–3276.

(29) Løvvik, O. M.; Opalka, S. M. *Surf. Sci.* **2008**, *602*, 2840.

(30) Hendriksen, B. L. M.; Bobaru, S. C.; Frenken, J. W. M. *Surf. Sci.* **2004**, *552*, 229.

(31) Piednoir, A.; Languille, M. A.; Piccolo, L.; Valcarcel, A.; Aires, F. J. C. S.; Bertolini, J. C. *Catal. Lett.* **2007**, *114*, 110.

(32) Chen, M.; Wang, X. V.; Zhang, L.; Tang, Z.; Wan, H. *Langmuir* **2010**, *26*, 18113.

(33) Hendriksen, B. L. M.; Ackermann, M. D.; van Rijn, R.; Stoltz, D.; Popa, I.; Balmes, O.; Resta, A.; Wermeille, D.; Felici, R.; Ferrer, S.; Frenken, J. W. M. *Nat. Chem.* **2010**, *2*, 730.

(34) van Rijn, R.; Balmes, O.; Felici, R.; Gustafson, J.; Wermeille, D.; Westerstroöm, R.; Lundgren, E.; Frenken, J. W. M. *J. Phys. Chem. C* **2010**, *114*, 6875.

(35) van Rijn, R.; Balmes, O.; Resta, A.; Wermeille, D.; Westerström, R.; Gustafson, J.; Felici, R.; Lundgren, E.; Frenken, J. W. M. *Phys. Chem. Chem. Phys.* **2011**, *13*, 13167.

(36) Hellman, A.; Resta, A.; Martin, N. M.; Gustafson, J.; Trinchero, A.; Carlsson, P.-A.; Balmes, O.; Felici, R.; van Rijn, R.; Frenken, J. W. M.; Andersen, J. N.; Lundgren, E.; Grönbeck, H. *J. Phys. Chem. Lett.* **2012**, *3*, 678.

(37) Toyoshima, R.; Yoshida, M.; Monya, Y.; Kousa, Y.; Suzuki, K.; Abe, H.; Mun, B. S.; Mase, K.; Amemiya, K.; Kondoh, H. *J. Phys. Chem. C* **2012**, *116*, 18691.

(38) Toyoshima, R.; Yoshida, M.; Monya, Y.; Suzuki, K.; Mun, B. S.; Amemiya, K.; Mase, K.; Kondoh, H. *J. Phys. Chem. Lett.* **2012**, *3*, 3182.

(39) Blomberg, S.; Hoffmann, M. J.; Gustafson, J.; Martin, N. M.; Fernandes, V. R.; Borg, A.; Liu, Z.; Chang, R.; Matera, S.; Reuter, K.; Lundgren, E. *Phys. Rev. Lett.* **2013**, *110*, 117601.

(40) Toyoshima, R.; Yoshida, M.; Monya, Y.; Suzuki, K.; Amemiya, K.; Mase, K.; Mun, B. S.; Kondoh, H. *J. Phys. Chem. C* **2013**, *117*, 20617.

(41) Westerström, R. et al. *Phys. Rev. B* **2011**, *83*, 115440.

(42) Rogal, J.; Reuter, K.; Scheffler, M. *Phys. Rev. Lett.* **2007**, *98*, 046101.

(43) Rogal, J.; Reuter, K.; Scheffler, M. *Phys. Rev. B* **2007**, *75*, 205433.

(44) Gao, F.; Wang, Y.; Cai, Y.; Goodman, D. W. *J. Phys. Chem. C* **2009**, *113*, 174.

(45) Zheng, G.; Altman, E. I. *J. Phys. Chem. B* **2002**, *106*, 1048.

(46) Méndez, J.; Kim, S. H.; Cerdá, J.; Wintterlin, J.; Ertl, G. *Phys. Rev. B* **2005**, *71*, 085409.

(47) Kim, S. H.; Méndez, J.; Wintterlin, J.; Ertl, G. *Phys. Rev. B* **2005**, *72*, 155414.

(48) Nakai, I.; Kondoh, H.; Shimada, T.; Resta, A.; Andersen, J. N.; Ohta, T. *J. Chem. Phys* **2006**, *124*, 224712.

(49) Nagarajan, S.; Thirunavukkarasu, K.; Gopinath, C. S. *J. Phys. Chem. C* **2009**, *113*, 7385.

(50) Gao, F.; McClure, S. M.; Cai, Y.; Gath, K. K.; Wang, Y.; Chen, M. S.; Guo, Q. L.; Goodman, D. W. *Surf. Sci.* **2009**, *603*, 65.

(51) Schnadt, J.; Knudsen, J.; Andersen, J. N.; Siegbahn, H.; Pietzsch, A.; Hennies, F.; Johansson, N.; Mårtensson, N.; Öhrwall, G.; Bahr, S.; Mähl, S.; Schaff, O. *J. Synchrotron Rad.* **2012**, *19*, 701.

(52) Doniach, S.; Šunjić, M. *J. Phys. C: Solid State Phys.* **1970**, *3*, 285.

(53) Perdew, J. P.; Burke, K.; Ernzerhof, M. *Phys. Rev. Lett.* **1996**, *77*, 3865.

(54) Kresse, G.; Hafner, J. *Phys. Rev. B* **1993**, *47*, 558.

(55) Kresse, G.; Hafner, J. *Phys. Rev. B* **1993**, *49*, 14251.

(56) Kresse, G.; Furthmüller, J. *Comput. Mater. Sci.* **1996**, *6*, 15.

(57) Blöchl, P. E. *Phys. Rev. B* **1994**, *50*, 17953.

(58) Kresse, G.; Joubert, D. *Phys. Rev. B* **1999**, *59*, 1758.

(59) Monkhorst, H. J.; Pack, J. D. *Phys. Rev. B* **1976**, *13*, 5188.

(60) Pack, J. D.; Monkhorst, H. J. *Phys. Rev. B* **1977**, *16*, 1748.

(61) Henkelman, G.; Jónsson, H. A dimer method for finding saddle points on high dimensional potential surfaces using only first derivatives. *J. Chem. Phys.* **1999**, *111*, 7010–7022.

(62) Carlsson, P.-A.; Skoglundh, M.; Thormählen, P.; Andersson, B. *Topics in Catalysis* **2004**, *30/31*, 375–381.

(63) Vogel, D.; Spiel, C.; Suchorski, Y.; Trinchero, A.; Schloegl, R.; Gronbeck, H.; Rupprechter, G. *Angew. Chem. Int. Ed.* **2012**, *51*, 10041.

(64) de Mongeot, F.; Rocca, M.; Valbusa, U. Energy and angle dependence of the initial sticking coefficient of $O_2$ on Ag(001). *Surface Science* **1996**, *363*, 68 – 72.

(65) Wang, C. P.; Yan, L. N.; Han, J. J.; Liu, X. J. *CALPHAD* **2012**, *37*, 57.

(66) The kinetic behavior is in qualitative agreement with the experimental data over the alloy surface for parameters in the ranges $E_a = [1.91 : 2.14], \nu^r = [10^{12} : 10^{17}], \alpha = [0.45 : 1.0]$ and $\beta = [0 : 0.5]$. The corresponding ranges for Pd(100) are $\nu^r = [10^{13} : 10^{16}], \alpha = [0.35 : 0.6]$ and $\beta = [0 : 0.4]$. $E_a$ is the barrier for Ag diffusion in the alloy.

(67) Todorova, M.; Lundgren, E.; Blum, V.; Mikkelsen, A.; Gray, S.; Gustafson, J.; Borg, M.; Rogal, J.; Reuter, K.; Andersen, J. N.; Scheffler, M. *Surf. Sci.* **2003**, *541*, 101.

(68) Fernandes, V. R.; Gustafson, J.; Farstad, M. H.; Walle, L. E.; Blomberg, S.; Lundgren, E.; Venvik, H. J.; Borg, A. *Appl. Surf. Sci.* **2014**, *313*, 794.

(69) Trinchero, A.; Hellman, A.; Gronbeck, H. *Surf. Sci.* **2013**, *616*, 206–213.

(70) Mavrikakis, M.; Hammer, B.; Norskov, J. Effect of strain on the reactivity of metal surfaces. *Phys. Rev. Lett.* **1998**, *81*, 2819–2822.

(71) Zorn, K.; Giorgio, S.; Halwax, E.; Henry, C. R.; Gronbeck, H.; Rupprechter, G. CO Oxidation on Technological Pd-Al2O3 Catalysts: Oxidation State and Activity. *J. Phys. Chem. C* **2011**, *115*, 1103–1111.

(72) Hauptmann, W.; Votsmeier, M.; Gieshoff, J.; Drochner, A.; Vogel, H. Inverse hysteresis during the NO oxidation on Pt under lean conditions. *Appl. Cat. B - Environmental* **2009**, *93*, 22–29.

(73) Hauff, K.; Tuttlies, U.; Eigenberger, G.; Nieken, U. Platinum oxide formation and reduction during NO oxidation on a diesel oxidation catalyst - Experimental results. *Appl. Cat. B - Environmental* **2012**, *123*, 107–116.

(74) Abedi, A.; aand M. Votsmeier, R. H.; Epling, W. S. *Catal. Lett.* **2012**, *142*, 930–935.

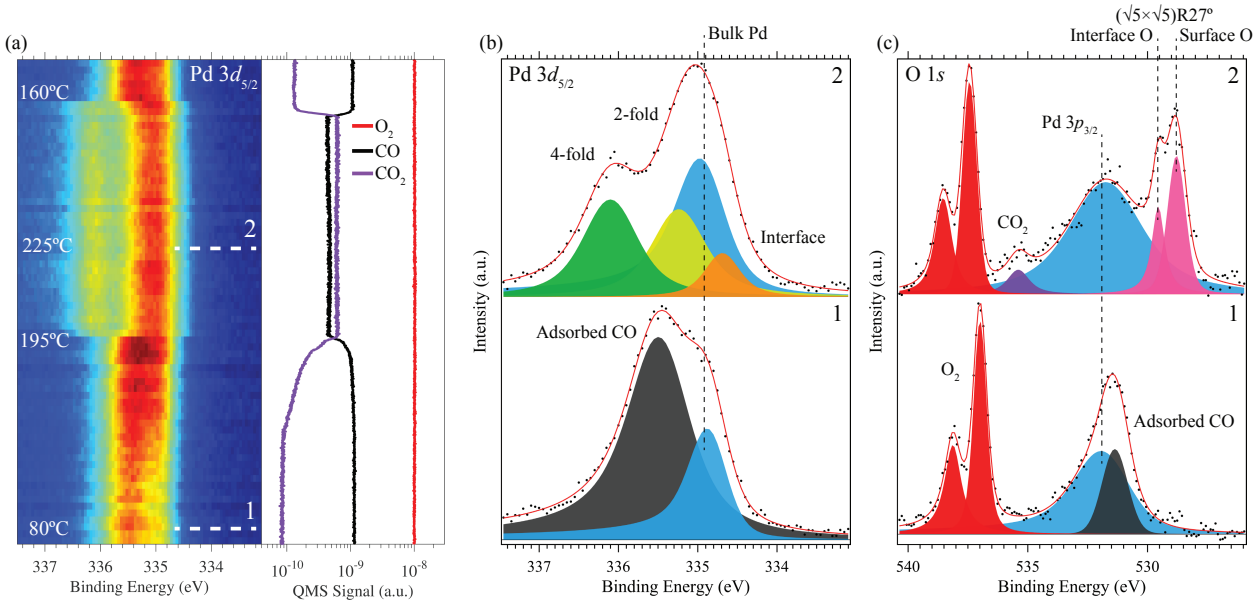


Figure 1: (a) *In situ* NAP-XPS measurements of the Pd $3d_{5/2}$ core level region along with QMS $O_2$, CO and $CO_2$ data recorded for CO oxidation over Pd(100) while ramping the sample temperature from about 80°C to 230 °C and down again to 155°C. (b) The Pd $3d_{5/2}$ core level spectra recorded at the beginning of the ramping series (lower panel, labeled 1) and at sample temperature 225°C (upper panel, labeled 2). (c) Corresponding O 1$s$ core level spectra measured for the CO covered surface (lower panel) and during $CO_2$ production (upper panel) for similiar ramping series as that shown in (a).

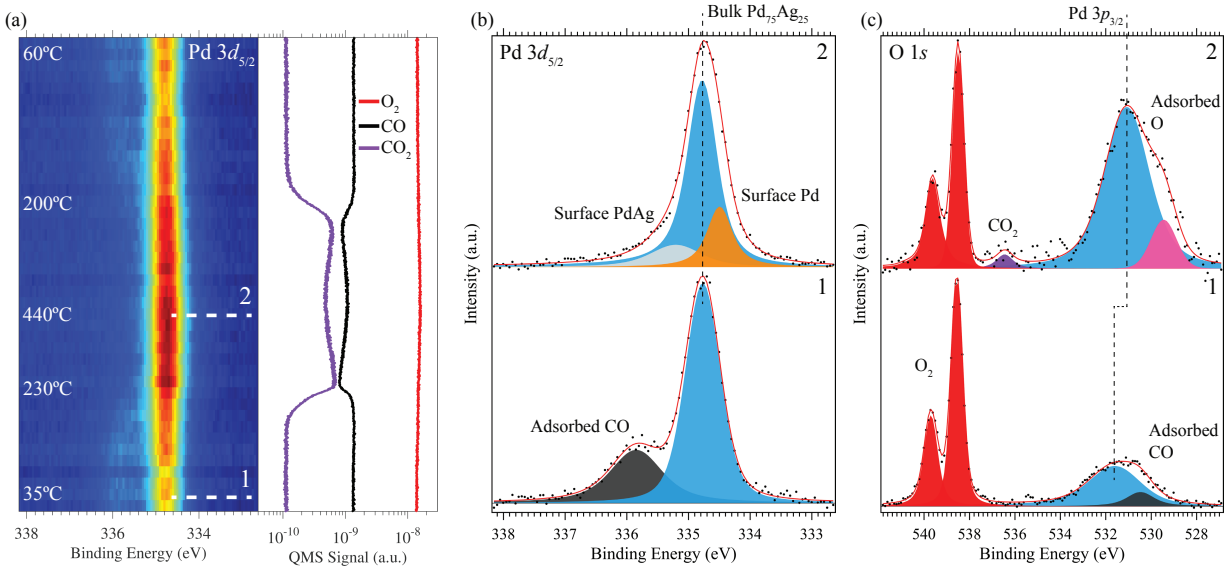


Figure 2: (a) *In situ* NAP-XPS measurements of the Pd $3d_{5/2}$ core level region along with QMS $O_2$, CO and $CO_2$ data recorded for CO oxidation over $Pd_{75}Ag_{25}(100)$ while ramping the sample temperature from about 35°C to 440°C and down again to 60°C. (b) The Pd $3d_{5/2}$ core level spectra recorded at the beginning of the ramping series (lower panel, labeled 1) and at sample temperature 440°C (upper panel, labeled 2). (c) Corresponding O $1s$ core level spectra measured for the CO covered surface (lower panel) and during $CO_2$ production (upper panel) for a similar ramping series as that shown in (a).

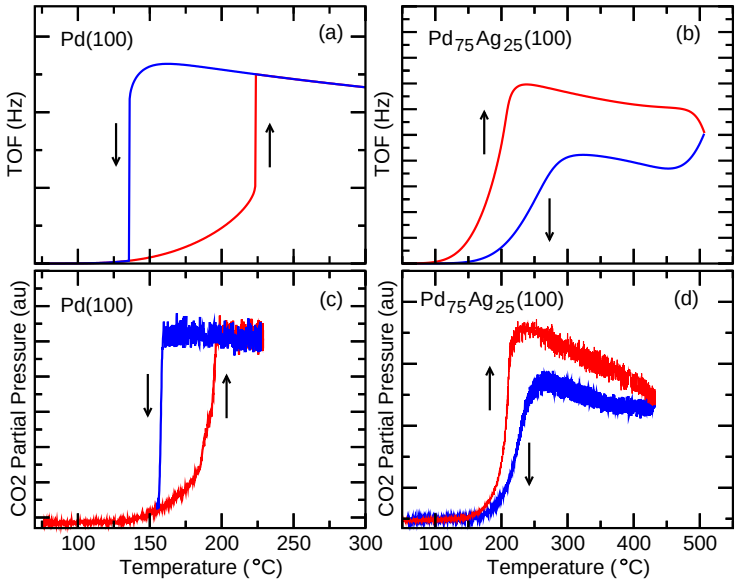


Figure 3: Measured $CO_2$ pressures and calculated turnover frequencies for temperature ramps over Pd(100) and $Pd_{75}Ag_{25}(100)$.

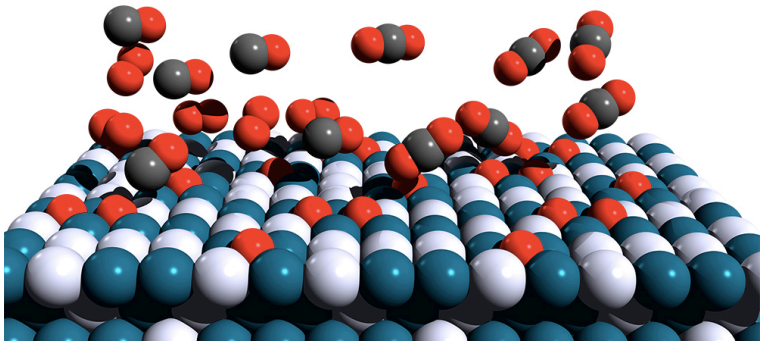

TOC graphics